Available online at www.sciencedirect.com
SCIENCE DIRECT®
International Journal of Mass Spectrometry 229 (2003) 209–216
International Journal of Mass Spectrometry
www.elsevier.com/locate/ijms

Nanoelectrospray ion mobility spectrometry and ion trap mass spectrometry studies of the non-covalent complexes of amino acids and peptides with polyethers

Michelle L. Colgrave, Claire J. Bramwell, Colin S. Creaser*

School of Science, Interdisciplinary Biomedical Research Centre, Nottingham Trent University, Clifton Lane, Nottingham NG11 8NS, UK

Received 29 July 2002; accepted 9 July 2003

Abstract

The non-covalent complexes formed between cyclic (e.g., 12-crown-4 (12C4), 15-crown-5 (15C5), and 18-crown-6 (18C6)) and acyclic (e.g., triglyme and tetraglyme) polyethers with amino acids (histidine and arginine) and peptides (MRFA, MFAR, gp70 and bradykinin) have been analysed by atmospheric pressure nano-electrospray ionisation (nano-ESI) ion mobility spectrometry and ion trap mass spectrometry. The reduced mobilities for these complexes are reported and correlate well with the mass and size of the polyether. The ability of IMS to distinguish between cyclic and acyclic polyethers and their complexes with biomolecules, based on differences in their reduced mobilities, is demonstrated. These differences are attributed to variations in the collision cross-section arising from subtle changes in conformation in these ligand–receptor complexes.

Keywords: Ion mobility spectrometry; Mass spectrometry; Peptides; Polyethers

1. Introduction

The mobility of a gas-phase ion is determined by its velocity through a drift region under the influence of an electric field gradient [1] and in the presence of a neutral buffer gas. Ions are gated into the drift region and are accelerated by the electric field, but slowed by collisions with the buffer gas, resulting in a constant drift velocity, v_d, which is proportional to the electric field gradient, E. The constant of proportionality between the drift velocity and the electric field gradient is the ion mobility, K, as shown in Eq. (1):

$$v_d = KE \quad (1)$$

Ion mobility depends on the charge, mass and collision cross-section of the ion. Hence, a large ion will undergo more collisions with the buffer gas than will an ion with a smaller collision cross-section, resulting in a lower mobility for the ion. Isomeric and isobaric compounds of the same charge may therefore be distinguished based upon differences in their collision cross-section.

Ion mobility measurements have been used to examine the gas-phase conformations of biomolecules including peptides and proteins following electrospray ionisation (ESI). Clemmer and Jarrold [2] have reviewed the use of IMS to deduce structural information, including the applications to large polyatomic species, such as clusters and biomolecules. The biomolecules examined by ESI-IMS include the proteins cytochrome *c*, bovine pancreatic trypsin inhibitor (BPTI), apomyoglobin, lysozyme and ubiquitin. Recent developments in the field of ion mobility spectrometry include the coupling of liquid chromatography (LC) [3,4] to IMS-quadrupole MS and IMS-TOF-MS configurations for the analysis of peptides and protein digests. The LC/IMS/TOF-MS configuration is achievable because of the differences in the time scales for each of the components of the experiment, i.e., minutes for HPLC/LC, milliseconds for IMS and microseconds for time-of-flight mass spectrometry (TOF-MS) [4].

The non-covalent interactions occurring between crown ether receptors and amino acid or peptide ligands are of interest as they act as simple models for biomolecular

* Corresponding author. Tel.: +44-115-8486657; fax: +44-115-8486636.
E-mail address: colin.creaser@ntu.ac.uk (C.S. Creaser).

1387-3806/$ – see front matter © 2003 Elsevier B.V. All rights reserved.
doi:10.1016/S1387-3806(03)00339-7

ligand–receptor interactions and aid in the understanding of molecular recognition in complex biological processes. The selectivity observed for macrocycles may be rationalised by consideration of the cavity size of the receptor and the size of the ligand or metal ion [5] as well as the importance of hydrogen bonding interactions [6]. Previous studies on 15C5 and 18C6 show that they bind cationic species in solution [7,8] and in the gas phase [5,6,9]. A recent report on the binding of 18C6 to lysine, proline, glycine, alanine, polylysine and small model peptides [10] demonstrated the role of the polyethers in the stabilisation of charge. The non-covalent adduct formation between 18C6 and mixtures of peptides and proteins has been utilised for the mass and charge assignment of the components of the mixtures in the ESI mass spectra [11]. Wyttenbach et al. [12] utilised MALDI-IMS and molecular dynamics simulations to examine the conformations of alkali ion cationised polyethers and found there to be good agreement between the experimental and theoretical cross-sections. The stability of the non-covalent inclusion complexes formed between crown ethers and a variety of protonated amines has also been explored by quadrupole ion trap mass spectrometry [13] and the non-covalent complexes of cyclic and acyclic polyethers with protonated amines and amino acids have been studied by atmospheric pressure IMS [14] and in a low pressure drift cell (<10 Torr He) using a tandem quadrupole ion trap/ion mobility spectrometer. [15,16] In both studies, IMS was able to distinguish between the complexes formed between the polyethers and isomeric amines.

We have recently described the design and coupling of a nanoelectrospray ionisation (nano-ESI) source to an atmospheric pressure ion mobility spectrometer [17]. The advantages of this configuration over conventional electrospray include lower sample consumption, longer sampling times and enhanced desolvation. We describe here the utility of the nano-ESI source coupled to the ion mobility spectrometer for the analysis of non-covalent ligand–receptor complexes of polyethers with a variety of amino acids and peptides.

2. Experimental

Experiments were performed using an atmospheric pressure ion mobility spectrometer (Smiths Detection, Watford, UK) that has been modified to incorporate a nano-ESI source [17]. The instrument was operated at 100 °C with an electric field gradient of 200 V cm^{-1}. High purity nitrogen (BOC Gases, Guildford, UK) was used as the buffer gas at a flow rate of 400 ml min^{-1}. Data was acquired using Trimscan^{TM} software (Graseby Dynamics, Watford, UK) at a sampling rate of 50 kHz with a repetition rate of 30 ms and a pulse width of 50 μs. The crown ethers (Fig. 1), 12-crown-4 (12C4), 15-crown-5 (15C5) and 18-crown-6 (18C6), and their acyclic analogues, triglyme (T_3G) and tetraglyme (T_4G) (CH_3–(CH_2CH_2O–)$_n$$CH_3$, n = 3–4) were obtained from Sigma-Aldrich Chemicals (Poole, UK) and used without further purification. The amino acids, L-histidine and L-arginine, and the peptides, MRFA, gp70 and bradykinin, were also purchased from Sigma-Aldrich Chemicals and used without further purification. The tetrapeptide, MFAR, was synthesised by John Keyte of the School of Biomolecular Sciences at the University of Nottingham (Nottingham, UK). Single letter designations for amino acids are used to describe peptide sequences.

For the initial examination of the free biomolecules, 5 μl of each of the amino acid and peptide solutions (10 mM in 50% acetonitrile/water + 1% acetic acid) were loaded into prebroken borosilicate capillaries (New Objective, Woburn, MA, USA) and analysed first by ion mobility spectrometry and then using a Finnigan LCQ ion trap quadrupole mass spectrometer (Thermo-Finnigan, Hemel Hempstead, UK). A nitrogen gas pressure of 2–10 psi was applied to the nano-ESI tips to initiate the electrospray. Reactions between the biomolecules and the polyethers were carried out in capillary by first loading 2 μl of a 10 mM solution of the amino acid or peptide and then adding 2 μl of the polyether (50 mM) to the capillary. In this manner, the reactions were monitored as the solutions mixed within the capillary. The instrumental settings described by Julian and Beauchamp [10] were utilised for the detection of the complexes by

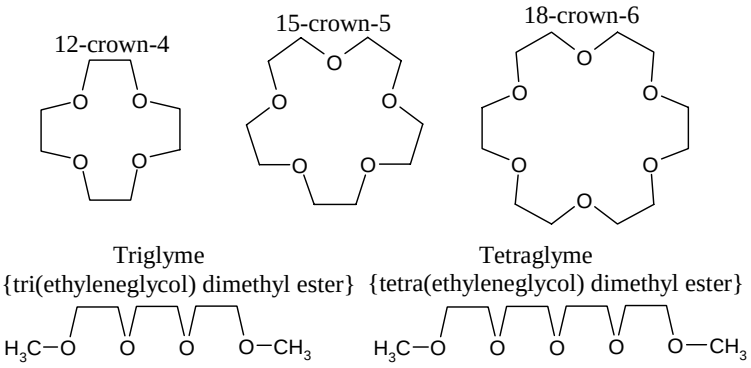

Fig. 1. Structures of the polyethers.

mass spectrometry. The free polyethers were also analysed by IMS and MS. The mobilities of the ions analysed by IMS were determined from the time taken for the ions to migrate along the drift cell (drift time, t_d) whilst under the influence of the weak electric field gradient in the presence of nitrogen buffer gas. The reduced mobilities were determined relative to 2,4-lutidine (2,4-dimethylpyridine) [18] using Eq. (2) to correct for variations in temperature and pressure:

$$K_0 = \frac{\text{drift time}_{\text{2,4-lutidine}}}{\text{drift time}_{\text{analyte}}} \times 1.950\,\text{cm}^2\,\text{V}^{-1}\,\text{s}^{-1} \quad (2)$$

The collision cross-sections were calculated using Eq. (3):

$$\Omega_D = \frac{3ze}{16N}\left[\frac{2\pi}{\mu kT}\right]^{1/2}\frac{1}{K_0} \quad (3)$$

where Ω_D is the collision cross-section; z is the charge on the ion; e is the unit of electronic charge; N is the number density of the buffer gas; k is the Boltzmann constant; T is the absolute temperature; μ is the reduced mass of the ion and K_0 is the reduced mobility.

3. Results and discussion

Solutions of the amino acids L-histidine (His) and L-arginine (Arg) (10 mM) were analysed by nano-ESI ion mobility spectrometry (nano-ESI-IMS) alone and following the addition of the cyclic polyethers, 12C4, 15C5 and 18C6 to the nano-ESI capillary. The free amino acids, His and Arg, were observed in the singly charged state with drift times of 9.08 and 9.53 ms corresponding to reduced mobilities of 1.675 and 1.596 $\text{cm}^2\,\text{V}^{-1}\,\text{s}^{-1}$, respectively, at 100 °C. Ion mobility spectra following addition of the crown ethers showed peaks assigned to the protonated amino acid/polyether complexes with drift times in the range of 12.5–14.8 ms. As the mixing of the polyethers and amino acids proceeded within the capillary, the peaks for the singly protonated forms of the free crown ether and the amino acid crown ether complex increased in intensity. The calculated reduced mobilities and collision cross-sections for the free polyether and amino acid–polyether ligand–receptor complexes are given in Table 1. The mass spectra (not shown) for the reaction mixtures confirmed the identities of the species observed in the IMS spectra.

Table 1
Reduced mobilities ($\text{cm}^2\,\text{V}^{-1}\,\text{s}^{-1}$) and collision cross-sections (Å^2) for the His and Arg complexes formed with 12-crown-4, triglyme, 15-crown-5, tetraglyme and 18-crown-6

Polyether (MW)	Free polyether		His complex (157.1)		Arg complex (174.2)	
	K_0	Ω_D	K_0	Ω_D	K_0	Ω_D
12C4 (176.2)	1.609	121.2	1.210	155.8	1.150	163.7
T_3G (178.2)	1.559	125.0	1.194	158.0	1.108	169.8
15C5 (220.3)	1.458	131.9	1.155	162.5	1.097	170.9
T_4G (222.3)	1.440	133.5	1.134	165.7	1.042	179.8
18C6 (264.3)	1.343	141.8	1.080	173.2	1.029	181.6

The mobilities of the free polyethers and polyether complexes were found to decrease as the size of the polyether was increased as a consequence of the increase in collision cross-section and mass-to-charge ratio. For example, the reduced mobility of the cyclic polyether–His complex decrease from 1.210 to 1.080 $\text{cm}^2\,\text{V}^{-1}\,\text{s}^{-1}$ as the polyether size increases from 12C4 to 18C6. The non-covalent complexes of L-histidine and L-arginine with the acyclic polyethers, triglyme (T_3G) and tetraglyme (T_4G) showed a similar trend with the K_0 for both of the free polyethers (T_3G = 1.559 $\text{cm}^2\,\text{V}^{-1}\,\text{s}^{-1}$; T_4G = 1.440 $\text{cm}^2\,\text{V}^{-1}\,\text{s}^{-1}$) and the amino acid complexes, e.g., His–T_3G (1.194 $\text{cm}^2\,\text{V}^{-1}\,\text{s}^{-1}$) and His–$T_4G$ (1.134 $\text{cm}^2\,\text{V}^{-1}\,\text{s}^{-1}$). The acyclic polyether complexes were also clearly distinguishable from those observed for the reactions between the amino acids and the corresponding cyclic analogues, 12C4 (free = 1.609 $\text{cm}^2\,\text{V}^{-1}\,\text{s}^{-1}$; His complex = 1.210 $\text{cm}^2\,\text{V}^{-1}\,\text{s}^{-1}$) and 15C5 (free = 1.458 $\text{cm}^2\,\text{V}^{-1}\,\text{s}^{-1}$; His complex = 1.155 $\text{cm}^2\,\text{V}^{-1}\,\text{s}^{-1}$). The differences observed result from an increased collision cross-section for the linear polyethers and their complexes with His (Table 1), from 155.8 Å^2 for His–12C4 to 158.0 Å^2 for His–T_3G and 162.5 Å^2 for His–15C5 to 165.7 Å^2 for His–T_4G confirming that in both cases the cyclic polyethers are able to adopt a more compact configuration than their acyclic analogues. Similar results were observed for the L-arginine ligand–receptor complexes with the cyclic and linear polyethers. The collision cross-sections calculated for the arginine complexes were greater than in all cases than those for the His complexes. These data are compared with the previous studies in which the linear polyethers were found to have larger collision cross-sections than their cyclic analogues [15,16].

The tetrapeptide, MRFA, was utilised as a model peptide for binding studies with the polyethers. Fig. 2a shows the variation in IMS ion intensity with time for the protonated peptide, polyether and peptide–polyether complex ions as the MRFA and 15C5 solutions mixed in the nano-ESI tip. Initially two peaks were observed in the IMS spectrum at 10.18 and 16.78 ms, assigned to the protonated MRFA monomer and dimer, respectively (Fig. 2b). As the mixing proceeded, the peaks for the MRFA–15C5 adduct at 11.75 ms and the free polyether at 10.42 ms increased in intensity as shown in Fig. 2c. Fig. 2d shows the nano-ESI ion trap mass spectrum acquired on the resultant reaction mixture. The peaks observed at m/z 524.2, 1047.1 and 1570.1 correspond to the monomeric $[\text{MRFA} + \text{H}]^+$, dimeric $[(\text{MRFA})_2 + \text{H}]^+$ and trimeric $[(\text{MRFA})_3 + \text{H}]^+$ species. The drift time for the $[(\text{MRFA})_3 + \text{H}]^+$ ion was greater than 20 ms and is therefore not observed in Fig. 2. The peaks at m/z 372.7 and 743.6 are assigned to the $[\text{MRFA} + 15\text{C5} + 2\text{H}]^{2+}$ and $[\text{MRFA} + 15\text{C5} + \text{H}]^+$ ions. A small peak at m/z 238.1 was also observed and corresponds to the 15C5–ammonium complex (i.e., $[15\text{C5} + \text{NH}_4]^+$). An additional peak was observed at m/z 482.3 and assigned

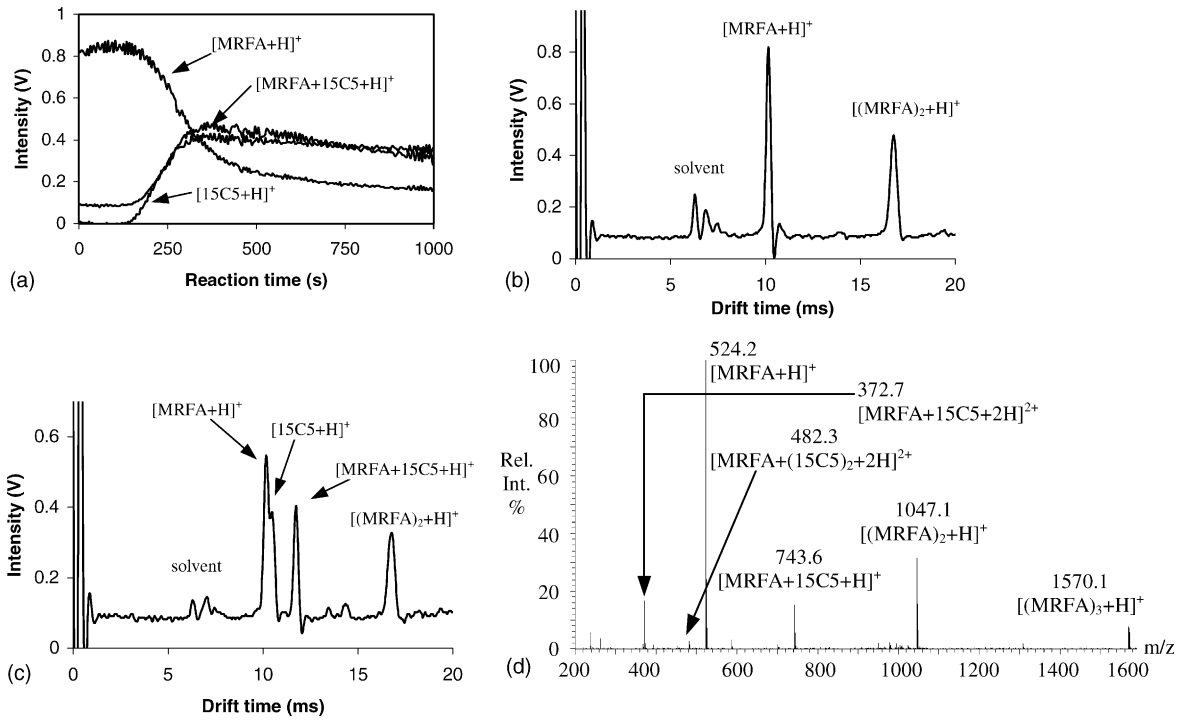

Fig. 2. Reaction between MRFA and 15-crown-5 monitored by ion mobility spectrometry and mass spectrometry. (a) Variation in ion intensity with drift time (ms) for the protonated peptide, polyether and polyether–peptide complex; (b) nano-ESI ion mobility spectrum of free MRFA; (c) nano-ESI ion mobility spectrum following the reaction between MRFA and excess 15C5; and (d) nano-ESI mass spectrum following reaction between MRFA and excess 15C5.

to the $[MRFA + (15C5)_2 + 2H]^{2+}$ species (i.e., with two bound polyethers present). It should be noted that ion mobility and mass spectra were recorded using the same sample, but in separate experiments. Mass spectral data were used only to confirm IMS peak assignments. The assignments of the IMS peaks for MRFA–15C5 are given in Table 2. Similar results were obtained for MRFA with 12C4, 18C6, T_3G and T_4G, after complete mixing of the two solutions, and the reduced mobilities and collision cross-sections are also summarised in Table 2.

The non-covalent complexes of the tetrapeptide, MFAR, an isomer of MRFA, were then investigated. The reaction of MFAR with the various polyethers resulted in the formation of two major products: a peptide–polyether complex and a peptide–$(polyether)_2$ complex. In the previous reactions with MRFA, the former was the major product, whilst the latter was only observed as a minor product. The increased abundance of $[MFAR + (polyether)_2 + H]^{2+}$ was evidenced by intense peaks in the nano-ESI mass spectra. For both MRFA and MFAR, there is a decrease in mobility and increase in collision cross-section with increasing polyether size. The change in cross-section for the linear and cyclic polyethers is much less marked than that observed for the amino acids histidine and arginine, but the trend for the linear polyether complexes to have a larger cross-section is followed for all but the 12C4 and T_3G complexes of MRFA.

Fig. 3a shows the nano-ESI ion mobility spectrum acquired following the reaction between MFAR and 15C5 and Fig. 3b shows the nano-ESI mass spectrum. The peaks at *m/z* 524.2 and 262.7 correspond to the $[MFAR + H]^+$ and

Table 2
Comparison of the reduced mobilities ($cm^2\,V^{-1}\,s^{-1}$) and collision cross-sections ($Å^2$) for the M + $(polyether)_n$ complexes (where M = MRFA or MFAR and $n = 1, 2$) formed upon binding of the polyether receptors to MRFA and MFAR

Polyether	MRFA		MFAR		Polyether	MRFA		MFAR	
	K_0	Ω_D	K_0	Ω_D		K_0	Ω_D	K_0	Ω_D
Free	1.495	124.4	1.478	125.8	Dimer	0.906	202.6	0.893	205.5
12C4	1.320	139.9	1.314	140.6	$(12C4)_2$	–	–	1.144	160.8
T_3G	1.322	139.7	1.313	140.7	$(T_3G)_2$	1.166	157.8	1.130	162.8
15C5	1.294	142.6	1.290	143.0	$(15C5)_2$	1.131	162.5	1.099	167.2
T_4G	1.291	142.9	1.285	143.6	$(T_4G)_2$	1.118	164.3	1.080	170.1
18C6	1.270	145.1	1.267	145.5	$(18C6)_2$	1.089	168.5	1.057	173.6

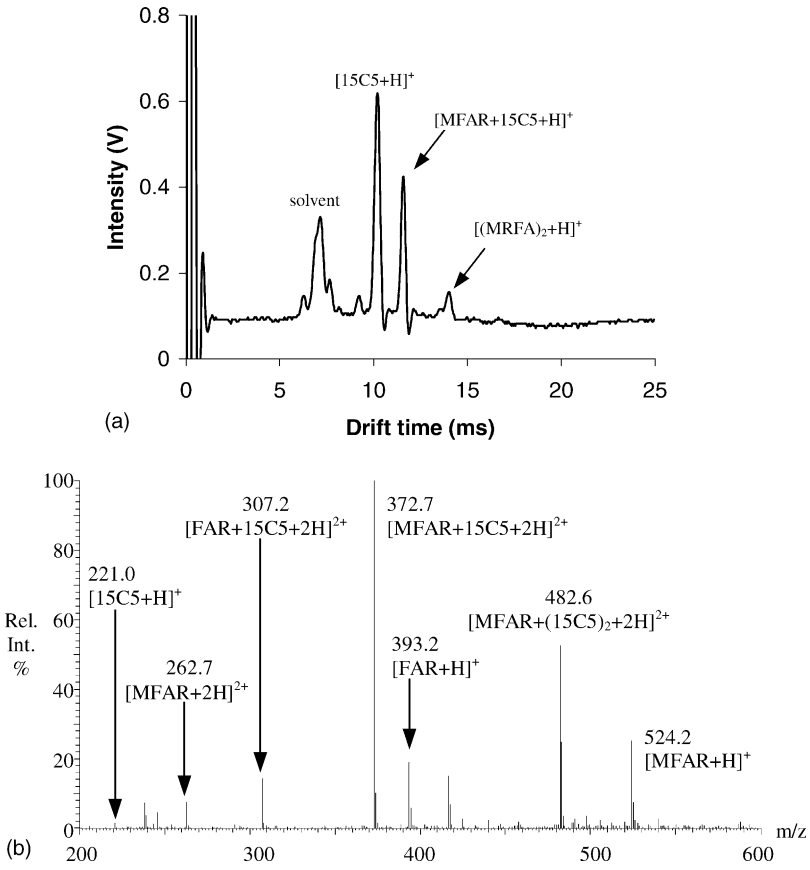

Fig. 3. Reaction between MFAR and excess 15-crown-5. (a) nano-ESI ion mobility spectrum at 100 °C and (b) nano-ESI mass spectrum.

$[MFAR + 2H]^{2+}$ species of the free tetrapeptide, whilst the small peaks at *m/z* 221.0 and 238.1 are assigned to the protonated species, $[15C5 + H]^+$, and the ammonium complex, $[15C5 + NH_4]^+$, of the polyether, 15C5. The large peak at *m/z* 372.7 corresponds to the $[MFAR + 15C5 + 2H]^{2+}$ ion, whilst the peak at *m/z* 482.6 represents the $[MFAR + (15C5)_2 + 2H]^{2+}$ complex ion. Two other peaks are also present in the nano-ESI mass spectrum: the peak at *m/z* 393.2 is derived from the failure sequence resulting from the peptide synthesis, i.e., the $[FAR + H]^+$ ion and the peak at *m/z* 307.2 corresponds to its 15C5 adduct, i.e., the $[FAR + 15C5 + 2H]^{2+}$ ion.

It is interesting to note that the difference in the reduced mobilities of the free tetrapeptides, MRFA ($1.495\,cm^2\,V^{-1}\,s^{-1}$) and MFAR ($1.478\,cm^2\,V^{-1}\,s^{-1}$) is $>0.01\,cm^2\,V^{-1}\,s^{-1}$, but on binding of the polyethers, there is a significant, but smaller difference in the mobilities ($0.003–0.009\,cm^2\,V^{-1}\,s^{-1}$). Nevertheless, in all cases the ion mobilities were sensitive to peptide sequences with the MFAR–polyether complexes showing higher collision cross-sections than their isomeric species. For example, the $[MRFA + 15C5 + H]^+$ ion has a collision cross-section of $142.6\,Å^2$ compared to $143.0\,Å^2$ for the $[MFAR + 15C5 + 2H]^+$ ion. Both MRFA and MFAR possess two possible sites of polyether binding: the N-terminal residue and the arginine side-chain. In the MRFA, these sites are adjacent, whilst in MFAR they are separated by three residues. It was therefore of interest to examine the formation of a M + (polyether)$_2$ species (where M = peptide), i.e., one in which two polyethers are bound to a single peptide. Table 2 summarises the reduced mobilities and collision cross-sections for these complexes.

The reduced mobilities of the MFAR + (polyether)$_2$ complexes were significantly lower than those of MRFA + (polyether)$_2$. For example, the MFAR + (15C5)$_2$ ion had a reduced mobility of $1.099\,cm^2\,V^{-1}\,s^{-1}$ and a calculated collision cross-section of $167.2\,Å^2$ compared to a reduced mobility of $1.131\,cm^2\,V^{-1}\,s^{-1}$ and collision cross-section of $162.5\,Å^2$ for the MRFA + (15C5)$_2$ ion. This indicates that steric repulsion of the bulky polyethers attached at the terminal sites in MFAR significantly increases the collision cross-section compared to MRFA, in which the polyethers are associated with adjacent amino acid residues and are therefore forced into a more compact conformation.

The study was extended to an examination of two larger peptides, the MHC Class I associated peptide, gp70 (SPSYVYHQF) and bradykinin (RPPGFSPFR). gp70 contains one basic amino acid side-chain (His), which along with the N-terminal amino group offer two possible sites for polyether binding. Bradykinin contains two basic amino acid side-chains (Arg) and an N-terminal amine and hence has three possible binding sites. Fig. 4a shows the IMS spec-

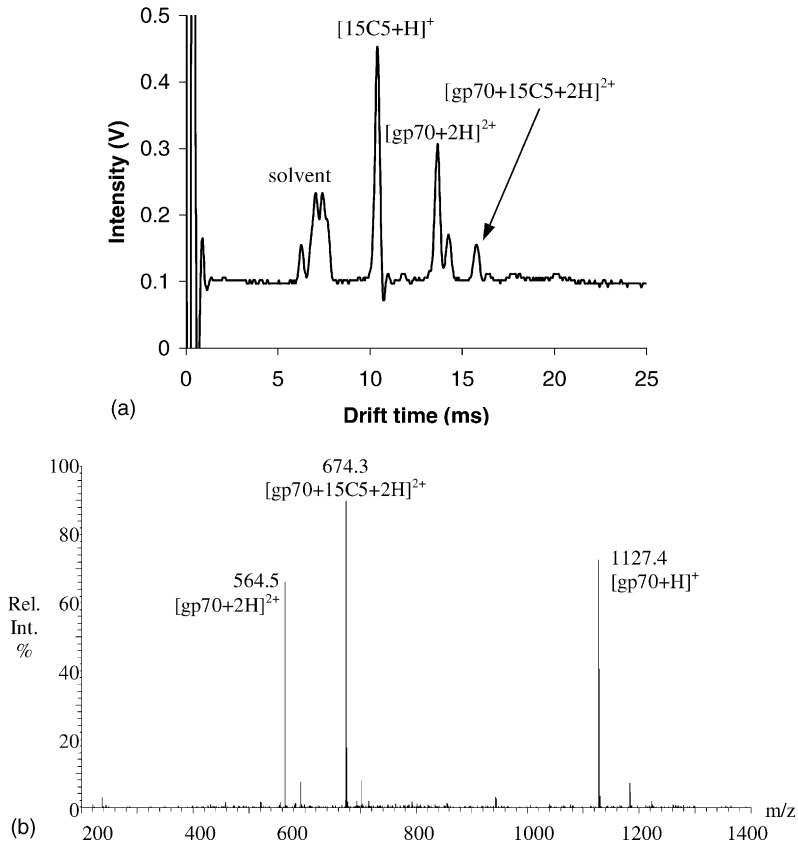

Fig. 4. Reaction between gp70 and excess 15-crown-5. (a) nano-ESI ion mobility spectrum at 100 °C and (b) nano-ESI mass spectrum.

trum of the reaction between gp70 and 15C5 and the corresponding mass spectrum is given in Fig. 4b. Fig. 5 shows the IMS and mass spectra acquired for the reaction between bradykinin and 15C5. The predominant peaks with drift times <25 ms, observed in the IMS spectra of both peptides in the absence of the crown ether, were the doubly protonated peptide $[M + 2H]^{2+}$ ions. On reaction with the polyethers, attenuation of these peaks occurred and peaks derived from the free polyethers and the polyether–peptide complexes increased in intensity. The reduced mobilities and calculated collision cross-sections are given in Table 3.

Fig. 4a shows the nano-ESI ion mobility spectrum obtained when the peptide gp70 was allowed to react with 15C5. A cluster of peaks is observed at ∼7.3 ms due to the solvent. The intense peak at 10.42 ms is assigned to the protonated crown ether. The peak at 13.65 ms is assigned to the doubly charged ion of the peptide, gp70. Both of these peaks identities have been confirmed by separate analysis of the species by IMS and ion trap mass spectrometry (Fig. 4b). The peak at 15.73 ms is assigned to the $[gp70+15C5+2H]^{2+}$ adduct formed between the polyether and the peptide. The mass spectrum of the reaction mixture between gp70 and 15C5 (Fig. 4b) confirms these assignments showing two peaks at *m*/*z* 564.5 and 1127.4 assigned to the $[gp70 + 2H]^{2+}$ and $[gp70 + H]^{+}$ species. The latter species was not observed in the IMS spectrum as the drift time was greater than 25 ms. The strong peak at *m*/*z* 674.3 is assigned to the $[gp70 + 15C5 + 2H]^{2+}$ ion. Three peaks of low intensity are also observed at *m*/*z* 592.5, 702.4 and 1183.4, which correspond to the *t*-butyl protected peptide (a minor contaminant from synthesis) and its complex with 15C5.

Table 3
Reduced mobilities ($cm^2\ V^{-1}\ s^{-1}$) and collision cross-sections ($Å^2$) for ligand–receptor complexes for the $[M+polyether+2H]^{2+}$ species where M = gp70 or bradykinin

Peptide	K_0/Ω_D	Free	12C4	T_3G	15C5	T_4G	18C6
gp70	K_0	1.114	1.001	–	0.967	0.960	0.962
	Ω_D	325.2	365.7	–	378.5	381.2	380.3
Bradykinin	K_0	1.139	1.020	1.009	1.009	0.993	0.996
	Ω_D	322.2	359.1	363.0	362.9	368.7	367.5

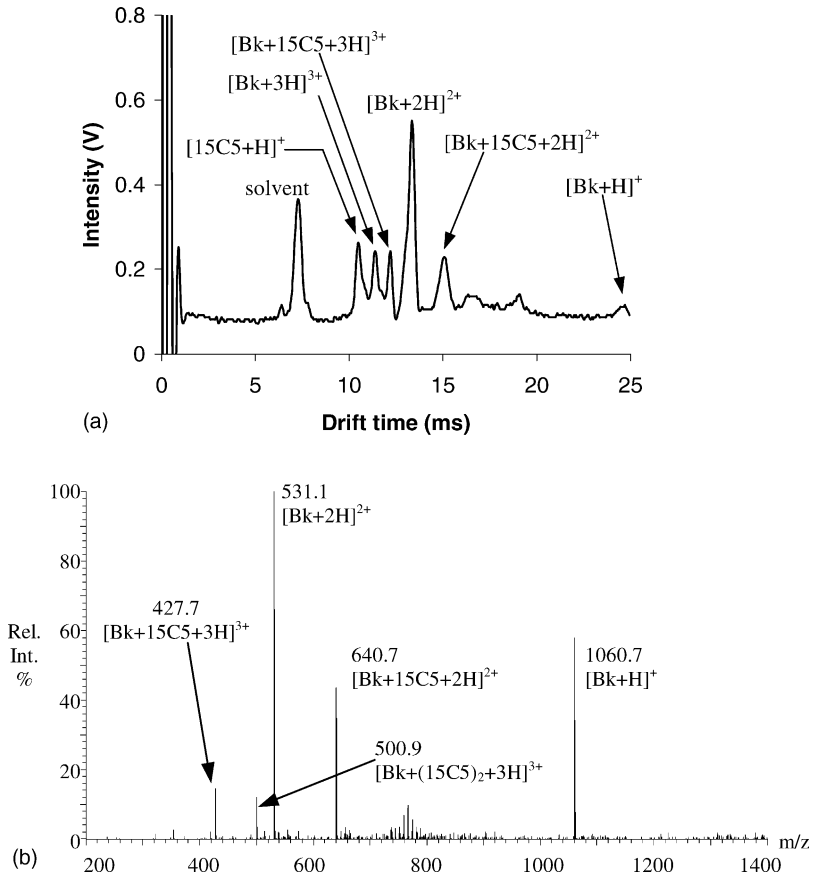

Fig. 5. Reaction between bradykinin and excess 15-crown-5. (a) nano-ESI ion mobility spectrum at 100 °C and (b) nano-ESI mass spectrum.

Fig. 5a shows the nano-ESI-IMS spectrum of the reaction between bradykinin and 15C5. The IMS spectrum for bradykinin is more complex than for gp70 owing to the observation of multiply charged ions, i.e., $[Bk + 3H]^{3+}$, $[Bk + 2H]^{2+}$ and $[Bk + H]^{+}$ ions with drift times of 11.33, 13.35 and 24.50 ms, respectively, corresponding to collision cross-sections of 409.9, 322.2 and 296.4 Å^2, which are in close agreement with those reported by Hill and co-workers (<2% variation) [19]. On addition of 15C5, a peak at 10.42 ms appeared corresponding to the free protonated polyether. The peaks at 12.22 and 15.08 ms were assigned to the $[Bk + 15C5 + 3H]^{3+}$ complex and the $[Bk+15C5+2H]^{2+}$ complex, respectively, with corresponding collision cross-sections of 441.3 and 362.9 Å^2. In the nano-ESI-MS of the reaction mixture between bradykinin and 15C5 (Fig. 5b), there are two peaks at *m*/*z* 531.1 and 1060.7 arising from the $[Bk+2H]^{2+}$ and $[Bk+H]^{+}$ species. An intense peak at *m*/*z* 640.7 is also observed corresponding to the $[Bk + 15C5 + 2H]^{2+}$ complex and the peak at *m*/*z* 427.7 represents the $[Bk + 15C5 + 3H]^{3+}$ ion. Two additional peaks are observed in the ion trap mass spectra, but not in the IMS spectra, for the $[Bk + (15C5)_2 + 3H]^{3+}$ ion (*m*/*z* 500.9) and $[Bk + (15C5)_3 + 3H]^{3+}$ ion (*m*/*z* 574.1). Similar results were obtained for the reactions with the remaining polyethers and the results are given in Table 3. It is interesting to note that, despite the increased charge state and size of the peptide, the trend towards larger collision cross-sections for the linear $[M + \text{polyether} + 2H]^{2+}$ complexes, compared to their cyclic counterparts, is clearly observed for bradykinin. A surprising observation is that for both the bradykinin and the gp70 peptides, the collision cross-sections of the $[M + 18C6 + 2H]^{2+}$ complexes lie between those for the $[M + 15C5 + 2H]^{2+}$ and $[M + T_4G + 2H]^{2+}$ complexes. These observed differences in collision cross-section are important because they establish that subtle changes in the conformation of non-covalent peptide complexes can be detected by IMS for larger peptides. This suggests that similar conformational changes in biomolecular ligand–receptor interactions, for which the peptide–polyether complexes are model systems, may be explored using the IMS technique.

4. Conclusions

The ligand–receptor complexes of a range of cyclic and acyclic polyethers to amino acids and peptides have been investigated by nano-ESI-IMS and ion trap mass spectrometry. The reduced mobilities and collision cross-sections of the complexes are reported. The reduced mobilities decrease with increasing size of the polyether and were lower for the acyclic polyethers than for their cyclic analogues.

The peptides MRFA and MFAR form peptide + polyether and peptide + $(\text{polyether})_2$ complexes, but steric hindrance in MRFA, which has adjacent polyether binding sites, restricts access to the second binding site. The collision cross-section of the doubly-bound ion was significantly larger for MFAR, because steric repulsion of the bulky polyether substituents causes unfolding of the compact globular structure. Subtle changes in collision cross-section were also observed for the peptide–polyether complexes of gp70 and bradykinin. These observations suggest that conformational changes resulting from ligand–receptor interactions of biological significance may be explored by the IMS technique.

Acknowledgements

We acknowledge support from the Engineering & Physical Sciences Research Council and Smiths Detection.

References

[1] G.A. Eiceman, Z. Karpas, Ion Mobility Spectrometry, CRC Press, Boca Raton, FL, USA, 1994.
[2] D.E. Clemmer, M.F. Jarrold, J. Mass Spectrom. 32 (1997) 577.
[3] L.M. Matz, H.M. Dion, H.H. Hill Jr., J. Chromatogr. A 946 (2002) 59.
[4] S.J. Valentine, M. Kulchania, C.A. Srebalus-Barnes, D.E. Clemmer, Int. J. Mass Spectrom. 212 (2001) 97.
[5] S. Maleknia, J. Brodbelt, J. Am. Chem. Soc. 115 (1993) 2837.
[6] M. Meot-ner, J. Am. Chem. Soc. 105 (1983) 4912.
[7] G.W. Gokel (Ed.), Comprehensive Supramolecular Chemistry, vol. 1, Pergamon Press, Oxford, 1996.
[8] V. Rudiger, H.J. Schneider, V.P. Solov'ev, V.P. Kazachenko, O.A. Raevsky, Eur. J. Org. Chem. (1999) 1847.
[9] M.B. More, D. Ray, P.B. Armentrout, J. Am. Chem. Soc. 121 (1999) 417.
[10] R.R. Julian, J.L. Beauchamp, Int. J. Mass Spectrom. 210/211 (2001) 613.
[11] J.B. Cunniff, P. Vouros, J. Am. Soc. Mass Spectrom. 6 (1995) 1175.
[12] T. Wyttenbach, G. von Helden, M.T. Bowers, Int. J. Mass Spectrom. Ion Proc. 165/166 (1997) 377.
[13] B.L. Williamson, C.S. Creaser, Int. J. Mass Spectrom. Ion Proc. 188 (1999) 53.
[14] C.S. Creaser, J.R. Griffiths, Anal. Chim. Acta 436 (2001) 273.
[15] C.S. Creaser, J.R. Griffiths, B.M. Stockton, Eur. Mass Spectrom. 6 (2000) 213.
[16] C.S. Creaser, J.R. Griffiths, B.M. Stockton, in: E. Gelpi (Ed.), Advances in Mass Spectrometry, Wiley, Chichester, UK, 2001, p. 407.
[17] C.J. Bramwell, M.L. Colgrave, C.S. Creaser, Analyst 127 (2002) 1467.
[18] Z. Karpas, Anal. Chem. 61 (1989) 684.
[19] C. Wu, J. Klasmeier, H.H. Hill, Rapid Commun. Mass Spectrom. 13 (1999) 1138.